SEARCH FOR ALPHA DRIVEN TAEs AT LOWERED ION TEMPERATURE IN TFTR DT DISCHARGES

S.J. ZWEBEN, R.V. BUDNY, C.Z. CHENG, E.D. FREDRICKSON, G.Y. FU, D.R. MIKKELSEN, G.L. SCHMIDT, S.D. SCOTT, D.A. SPONG[a], C.E. BUSH, Z. CHANG, D.S. DARROW, R.J. FONCK[b], L.R. GRISHAM, E. MAZZUCATO, R. NAZIKIAN, D.K. OWENS, H.K. PARK, S.F. PAUL, J.F. SCHIVELL, J.D. STRACHAN, E.J. SYNAKOWSKI, G. TAYLOR, K.M. YOUNG
Princeton Plasma Physics Laboratory, Princeton University, Princeton, New Jersey

[a] Oak Ridge National Laboratory, Oak Ridge, Tennessee

[b] University of Wisconsin, Madison, Wisconsin

United States of America

ABSTRACT. An experiment was performed in TFTR DT plasmas in an attempt to destabilize the alpha particle driven toroidicity-induced Alfvén eigenmodes (TAEs) by reducing their thermal ion Landau damping. The thermal ion Landau damping was reduced by transiently lowering the ion temperature using either helium (He) gas puffs or deuterium (D) or lithium (Li) pellet injection during neutral beam injection (NBI) into DT supershots. The ion temperature was successfully lowered from $T_i(0) \approx 20$ keV to $T_i(0) \approx 10$ keV in about 0.2 s; however, no alpha driven TAEs were observed. Theoretical analyses of the TAE instability of these DT discharges indicate that the alpha pressure required for TAE stability still remained greater than that actually obtained in this experiment, mainly because of the effects of beam ion Landau damping.

1. INTRODUCTION

A potential problem for tokamak reactors concerns the deleterious effect of possible alpha particle driven instabilities such as the toroidal Alfvén eigenmodes (TAEs). The TAE is one type of global shear-Alfvén MHD eigenmode in a torus, which in theory can be driven unstable by the free energy associated with a sufficiently large pressure gradient of super-Alfvénic alpha particles [1–4].

Previous tokamak experiments in deuterium (DD) plasmas have studied TAEs that were driven unstable by fast ions from neutral beam injection (NBI) [5, 6] or ion cyclotron minority heating (ICRH) [7, 8]. These studies are being extended in TFTR to DT alpha particles, which have a higher energy and a more isotropic distribution function than either the NBI or ICRH fast ions. Although the alpha particle pressure in TFTR is ≈ 5 to 10 times smaller than the fast ion pressures previously obtained with NBI or ICRH, the alpha pressure gradient in TFTR is within about a factor of 3 of that expected for future alpha driven DT tokamak reactors such as ITER [9, 10].

In this TFTR 'supershot' regime the alpha particle pressure is highest for discharges with the highest DT fusion power. However, no clear signs of any alpha driven TAEs have been observed so far in these DT supershots up to 10.7 MW of fusion power [11–14].

The present experiment was motivated by an early analysis of TAE stability in TFTR DT [1], which suggested that the dominant TAE damping mechanism is ion Landau damping, which could be reduced by lowering the ion temperature or, more precisely, the ion beta (β_i). The present experiment was designed to reduce the ion temperature while maintaining the maximum possible alpha particle pressure. This was accomplished by transiently cooling a high fusion power supershot (similar to that described previously in Ref. [11]) with helium gas puffs or with deuterium or lithium pellet injection.

The result of this experiment is that no signs of any alpha driven TAEs were observed even when the ion temperature was lowered from $T_i(0) \approx 20$ keV to $T_i(0) \approx 10$ keV in about 0.2 s. Theoretical analyses of the TAE instability of these DT discharges indicate that the alpha pressure required for TAE stability still remained greater than that actually obtained in this experiment. This was largely due to three factors:

(a) These cooling perturbations caused the density profiles to evolve in such a way as to close the TAE gap structure for the most unstable modes ($n \geq 2$), thus leading to strong continuum damping not present before the cooling.

(b) The beam ion and electron Landau damping

TABLE I. TAE STABILITY PARAMETERS FOR DT BASELINE CASE
(TRANSP analysis of shot 73 268 at 3.8 s, no cooling perturbation)

$V_{\alpha 0} = 1.3 \times 10^9$ cm/s	DT alpha birth speed ($E = 3.5$ MeV)
$V_A(0) = 7 \times 10^8$ cm/s	Central Alfvén speed ($n_e = 7 \times 10^{13}$ cm^{-3}, $B = 5$ T, DT)
$V_{\alpha 0}/V_A(0) = 1.8$	Alpha birth speed/ central Alfvén speed
$V_i(0)/V_A(0) = 0.15$	Thermal ion speed/ central Alfvén speed ($T_i(0) = 25$ keV, $M = 2.5$)
$V_{bD}/V_A(0) = 0.45$	Deuterium neutral beam speed/ central Alfvén speed ($E_b = 100$ keV)
$V_{bT}/V_A(0) = 0.37$	Tritium neutral beam speed/ central Alfvén speed ($E_b = 100$ keV)
$\beta(0) = 3.6\%$	Total plasma beta on-axis
$\beta_\alpha(0) = 0.22\%$	Alpha beta on-axis
$\beta_i(0) = 1.8\%$	Thermal ion beta on-axis
$\beta_b(0) = 0.35\%$	Total beam ion beta on-axis

was significant, and was not reduced by the transient cooling of the thermal ions.

(c) The alpha particle beta was reduced by about a factor of 2 by classical thermalization during these cooling perturbations.

Thus, the theoretical predictions are consistent with the observed absence of alpha driven TAEs in this experiment.

The outline of this paper is as follows: the theoretical motivation is described in Section 2, the experimental scenarios are discussed in Section 3, the experimental results are presented in Section 4, the TAE stability analyses are presented in Section 5, and a discussion is given in Section 6, including a summary and suggestions for further work.

2. THEORETICAL MOTIVATIONS

The first analysis of alpha driven TAEs in a tokamak found the instability threshold by equating the

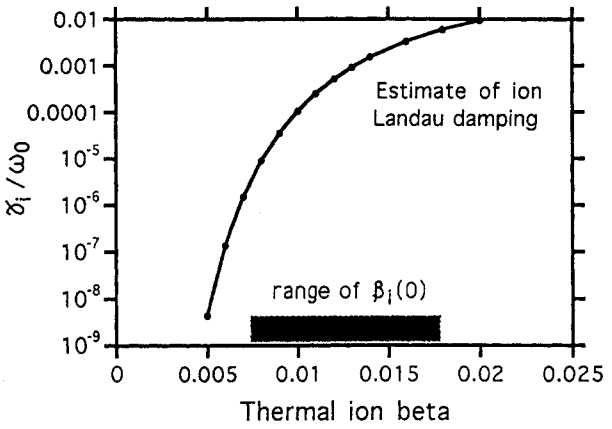

FIG. 1. Simplified theoretical dependence of the thermal Maxwellian ion Landau damping γ_i/ω_0 (normalized to the TAE frequency) on the ion beta. Ion Landau damping is expected to be very sensitive to the ion beta over the range of this experiment, indicated at the bottom of this figure.

'drive' from the local super-Alfvénic alpha particle pressure gradient with the local parallel electron damping [15]. It was soon recognized that this local β_α threshold for TAE instability should be exceeded in TFTR DT experiments [16].

Subsequently, increasingly realistic calculations for alpha driven TAEs in TFTR DT plasmas have been made by including the two dimensional eigenmode geometry, the finite alpha orbit widths and gyroradii, and additional damping mechanisms such as ion Landau damping and continuum damping. In general, these added effects have been stabilizing, such that the alpha driven TAEs are presently calculated to be stable in the highest powered TFTR DT discharges [2, 3, 12–14]. For example, when radiative damping [17, 18] was included, the total damping in normal TFTR supershots increased by about a factor of 2 between $n = 2$ and $n = 6$ [14].

A major reason for the stability of alpha driven TAEs in TFTR DT plasmas is ion Landau damping, which can be large in TFTR owing to its high ion temperature and pressure in the supershot regime. Ion Landau damping of TAEs in tokamaks is mainly caused by the poloidally varying magnetic drift velocity [15], which creates a new resonance at a third of the Alfvén speed V_A, which is coincidentally near the speed of thermal or beam ions in TFTR (Table I). In general, this resonance can either damp or drive the TAEs, depending on the shape of the distribution function. However, for TFTR supershots the dominant effect (by far) is for the thermal and beam ions to damp the TAE, rather than to drive it, whereas the

main drive is from the alpha particles near the primary resonance near V_A. In TFTR supershots, this thermal and beam ion damping is particularly important since the pressure of these ions is at least 5 times the alpha particle pressure (Table I).

A simple expression [19] for the thermal ion Landau damping rate γ_i, normalized to the TAE frequency ω_0, for a Maxwellian ion species is

$$\gamma_i/\omega_0 \approx 7 \times 10^{-3} q^2 \beta_i^{-3/2} \exp(-1/9\beta_i) \quad (1)$$

where β_i is the ion beta, which depends on both the ion temperature and the ion density. Therefore, the thermal ion Landau damping should strongly decrease if the central ion beta is reduced by a factor of 2 from its normal supershot value, as illustrated in Fig. 1.

Several detailed numerical studies of TFTR TAE stability were made prior to the DT run, on the basis of extrapolating a standard $I = 1.6$ MA deuterium-only NBI (DD) supershot to DT NBI using TRANSP. For these analyses the ions were simulated by a single species Maxwellian at the measured TFTR ion temperature of $T_i(0) \approx 20$ keV, i.e. no separate beam ion component was included, and the plasma parameters and profiles were taken to be the DD experimental values. Both the NOVA-K [1, 2] and the TAE/FL [3, 4] codes showed that ion Landau damping would be the dominant damping mechanism for low-n modes in TFTR supershots ($n = 1$–5). However, the calculated threshold for alpha driven TAEs was still a factor of 2 to 3 higher than the expected experimental alpha pressure, i.e. the alpha driven TAEs were predicted to be stable, largely owing to the effect of ion Landau damping.

The present experiment was motivated by these early theoretical studies, which suggested that the alpha driven TAE might be destabilized by reducing the ion Landau damping in TFTR DT supershots. In TFTR, the ion Landau damping can most easily be reduced by lowering the ion temperature, since the density cannot easily be lowered while maintaining a high alpha pressure, and the magnetic field was already near its maximum value.

Additional TAE simulations were performed to determine the effect of lowering the ion temperature in a standard DT supershot. The NOVA-K code simulated the effect of reducing the ion temperature using a scan of NBI heating power, self-consistently varying other parameters such as electron temperature, density and alpha particle beta. The result was that the TAE was predicted to be marginally unstable at an ion temperature of $T_i(0) \approx 10$ keV [1]. The TAE/FL code varied the ion temperature while holding all profiles and other parameters fixed, with the result that the total TAE damping rate was decreased by about a factor of 2 between $T_i(0) \approx 20$ keV and 10 keV. However, all of these calculations were sensitive to the plasma profiles, for example, through the radial variation of the TAE structure, alpha drive and damping rates. For example, the sensitivity of the TAE growth rate to $T_i(0)$ was found in TAE/FL to be much reduced for an $I_p = 1.8$ MA case run with the same toroidal field and beta as the original $I_p = 1.6$ MA case. This sensitivity was due to the change in $q(r)$ profile, which is known to affect continuum damping strongly [20].

Another physical motivation for this experiment was the theoretical observation that the global TAEs were often destroyed by large continuum damping near the plasma MHD beta limit [1, 21]. Since the standard high-powered TFTR supershots were near this beta limit, it was conjectured that the TAE instability threshold could be further reduced by lowering the total plasma beta. For example, NOVA-K analysis showed that although the alpha particle drive was highest at $P = 30$ MW of NBI, at that power the $n = 1$ TAEs were continuum damped because the plasma was approaching the MHD beta limit at $I_p = 1.6$ MA [1]. Note that these calculations did not include compressibility, which could modify the gap structure and the continuum (and radiative) damping [22, 23]; however, the beta in TFTR is low enough that the frequency shift is negligible.

These were the theoretical ideas and simulations that motivated the present experiment. The TAE stability calculations for the actual DT discharges used in this experiment are described in Section 5.

3. EXPERIMENTAL SCENARIOS

The goal of this experiment was to destabilize the alpha driven TAE by reducing the ion temperature, while at the same time keeping the TAE drive due to the alpha pressure gradient as high as possible. Normally these requirements are mutually exclusive, since the DT reactivity and the associated alpha pressure increase with ion temperature.

Several possible 'steady state' scenarios were considered to reconcile these requirements. One was to reduce the level of NBI power in a standard supershot, and another was to degrade the wall conditioning to form a high-power L mode plasma. Although both of these scenarios would have reduced the ion

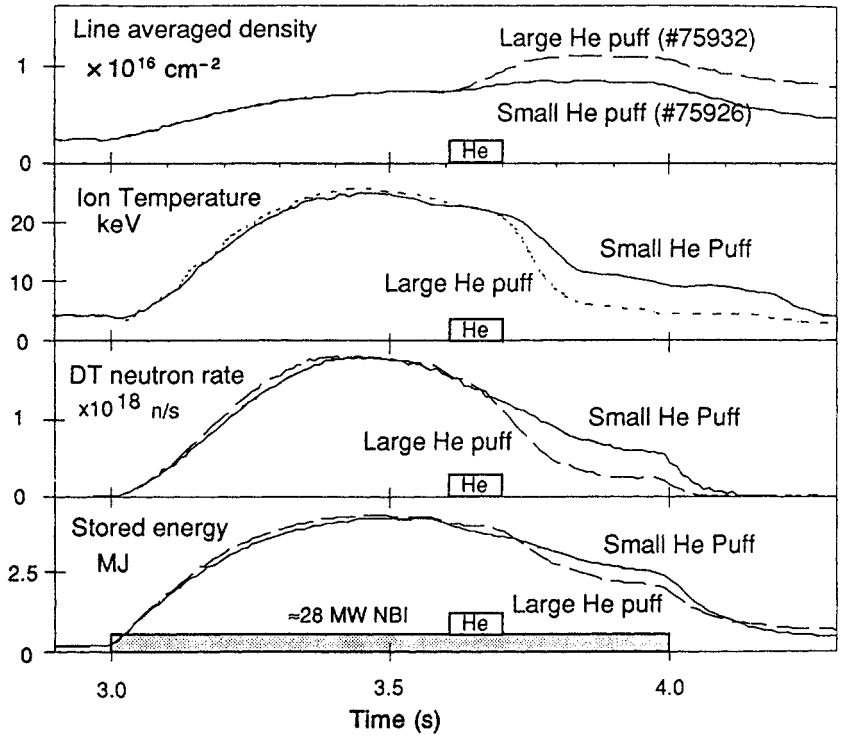

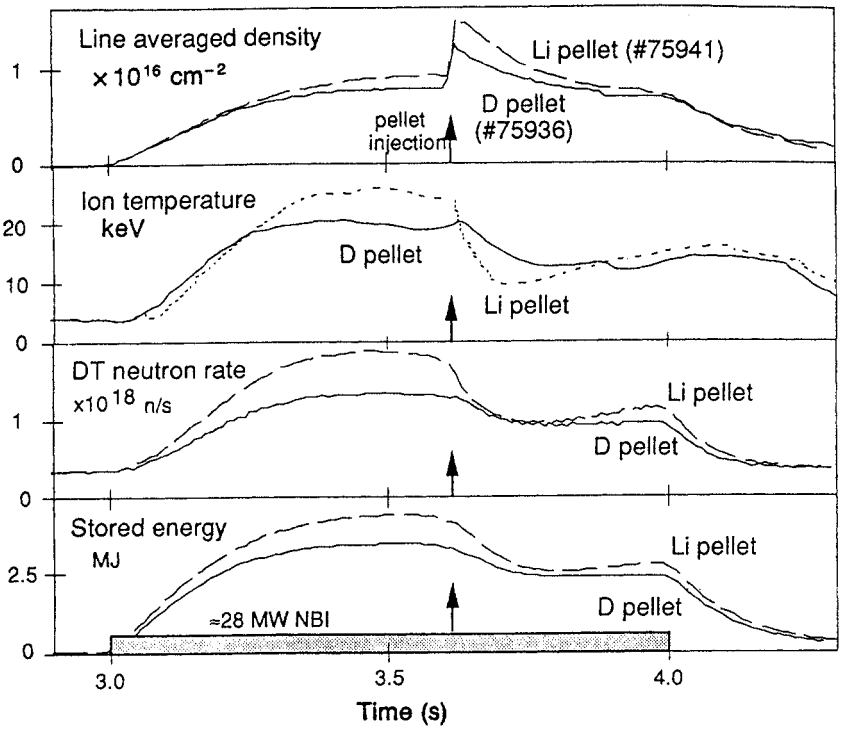

FIG. 2. Time dependences of line averaged density, ion temperature, DT neutron rate and total plasma stored energy for the four DT discharges in this experiment. The cooling perturbations began at 3.6 s in all cases. These perturbations changed a supershot plasma to an L mode plasma in ≈ 0.1 s. The time dependences of the companion DD plasmas were very similar.

temperature to $T_i(0) \approx 5$–10 keV, the DT reaction rates and alpha pressures were estimated to be a factor of ≈ 5 below that for high fusion power supershots, which was unacceptably low.

The alternative approach was a 'transient' scenario based on first establishing a large alpha population, and then rapidly cooling the ions before the alphas thermalized. Since the expected growth time of TAEs is relatively short (< 10 ms at $\gamma/\omega \approx 10^{-4}$ and $f \approx$ 300 kHz), and since the alpha thermalization time is normally very long (≈ 0.5 s) [18], it was acceptable to cool the ions on the energy confinement timescale of ≈ 0.1–0.2 s.

A simple transient scenario naturally occurs just after the NBI is turned off, when the ion temperature and beta drop faster than the alpha pressure [24]. Early theoretical analyses had suggested that this period could be TAE unstable [1], although the analysis was uncertain owing to the rapidly varying and incompletely diagnosed equilibrium and plasma profiles after NBI. However, no signs of any TAE instability have yet been observed during this time period [11–13].

The actual scenario used for the present experiment was to cool a high temperature DT supershot transiently using helium gas puffs or pellet injection during NBI. Earlier DD transport experiments in TFTR had shown that such supershots could be transformed into low ion temperature L mode discharges within ≈ 0.1 s [25]. It was estimated that about half the initial alpha pressure would remain 0.1 s after the cooling perturbation, despite the larger electron density and lower electron temperature after the cooling perturbations. Thus, the alpha pressure in this transient scenario would be considerably larger than that for the steady state scenarios.

The plasmas of the present experiment were similar to those used to obtain 6.3 MW of fusion power [11], i.e. $I_p = 2.0$ MA, $R = 2.52$ m and 30 MW NBI [11]. That previous 'baseline' DT discharge (No. 73 268) showed no signs of TAE instability, and was calculated to be stable to TAEs by both the NOVA-K and TAE/FL codes [2, 3]. The present DT discharges had a slightly lower NBI power and less lithium wall conditioning to avoid the disruptive beta limit, which was being approached in the baseline DT discharge.

4. EXPERIMENTAL RESULTS

There were four DT discharges in this experiment, each having a different type of transient ion cooling perturbation: one with a small helium gas puff (5.5 torr·L), one with a large helium gas puff (18 torr·L), one with a single deuterium pellet and one with a single lithium pellet. Each of these cooling perturbations began when the alpha particle pres-

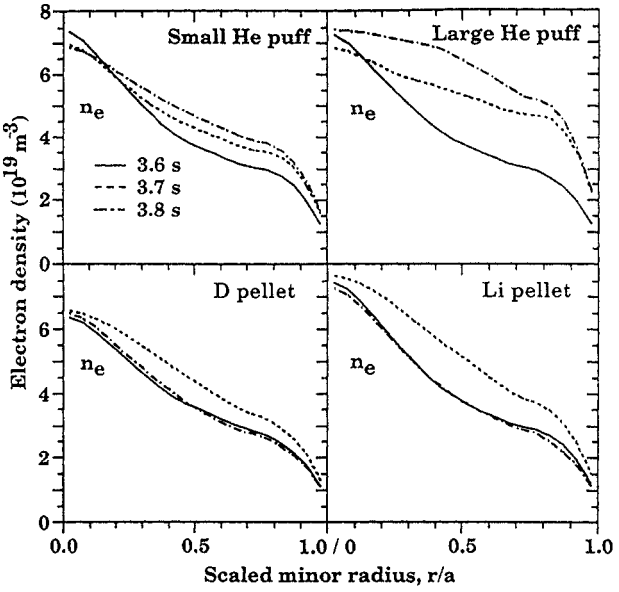

FIG. 3. Evolution of the electron density profiles for the DT discharges in this experiment, as measured by the multichannel interferometer. The density profiles broaden during these cooling perturbations, but the central densities were approximately unchanged.

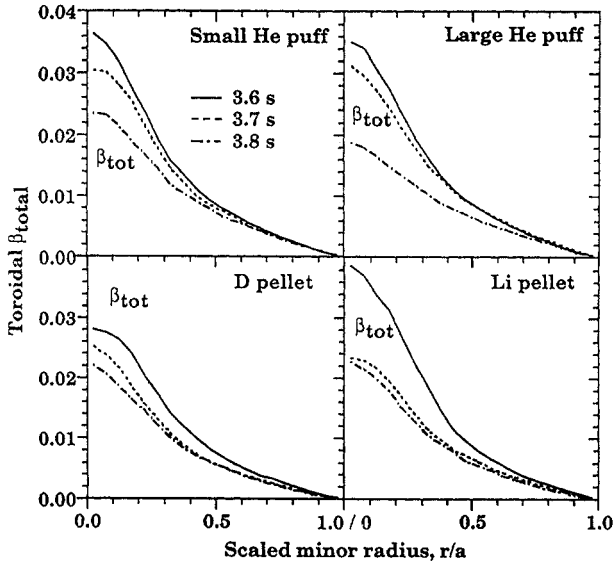

FIG. 4. Evolution of the total toroidal beta profiles for the DT discharges in this experiment, as calculated by TRANSP. The central beta decreased significantly, but the beta in the outer half of the plasma was changed less.

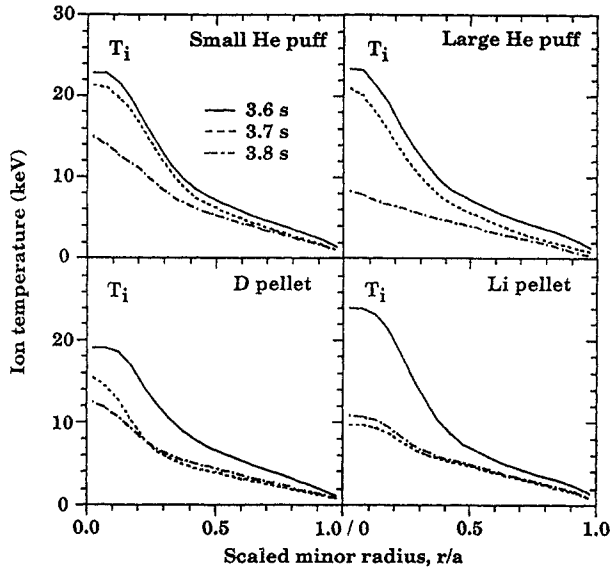

FIG. 5. Evolution of the ion temperature profiles for the DT discharges in this experiment, as measured by the CHERS diagnostic. The central ion temperatures fell from $T_i(0) \approx 19 - 23$ keV to $T_i(0) \approx 8 - 15$ keV during these discharges within 0.2 s after the start of the cooling perturbations.

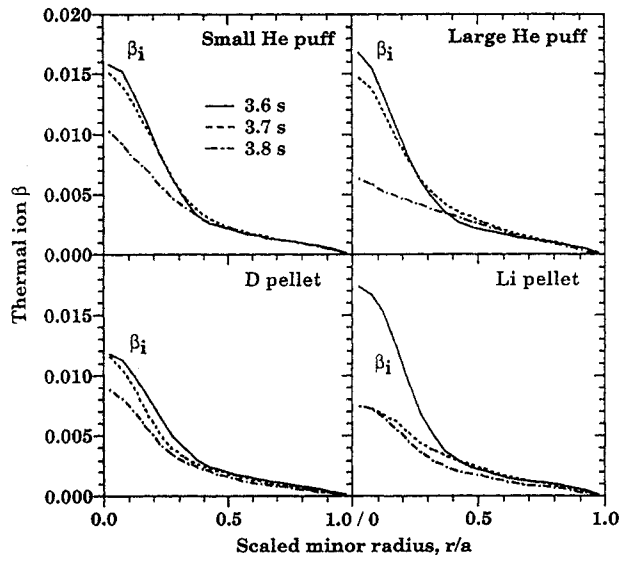

FIG. 6. Evolution of the thermal ion beta profiles for the DT discharges in this experiment, as calculated by TRANSP. The central thermal ion beta fell by up to a factor of ≈2 within ≈0.2 s after these cooling perturbations. However, the thermal ion betas at r/a ≥ 0.5 did not change significantly during this time, because of the rise in density associated with these cooling perturbations.

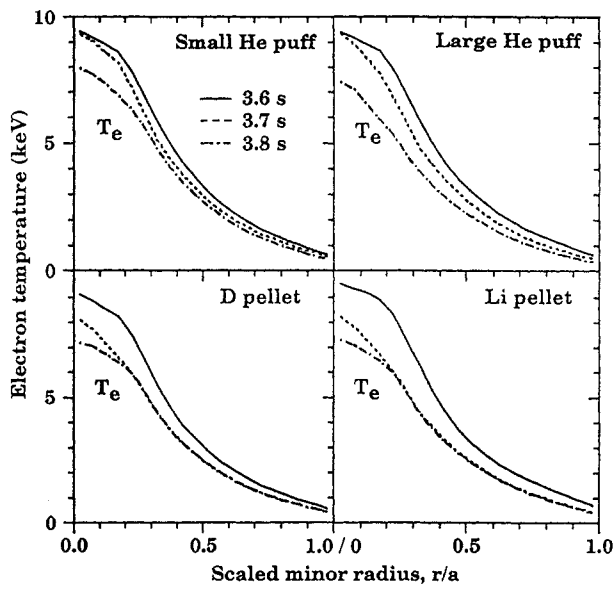

FIG. 7. Evolution of the measured electron temperature profiles for the DT discharges in this experiment, as measured by the ECE diagnostic. The temperature profiles were relatively unaffected during the ≈0.2 s after the start of these cooling perturbations.

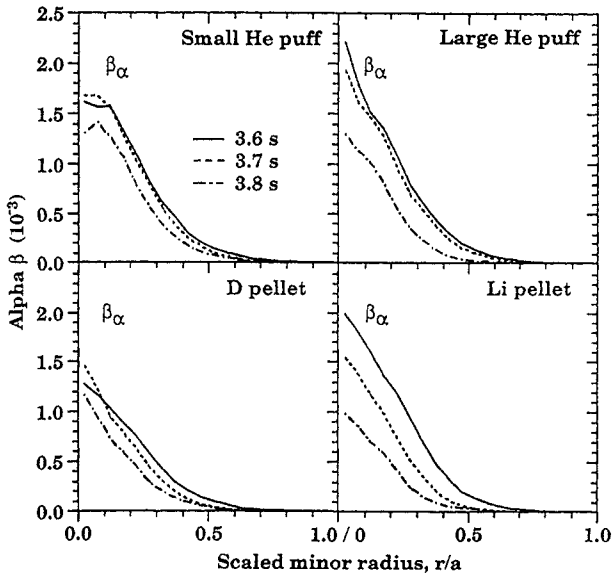

FIG. 8. Evolution of the alpha particle beta profiles of the DT discharges in this experiment, as calculated by TRANSP. These calculations assume classical alpha particle confinement and thermalization. The alpha particle betas fell by less than a factor of 2 during the ≈0.2 s after the start of these cooling perturbations. The ≈10% alpha loss due to TF ripple transport is not included.

sure was near its maximum, i.e. 0.6 s after the start of NBI. The main time of interest was 0.1 to 0.2 s after the start of the cooling perturbation when the alpha pressure still remained high.

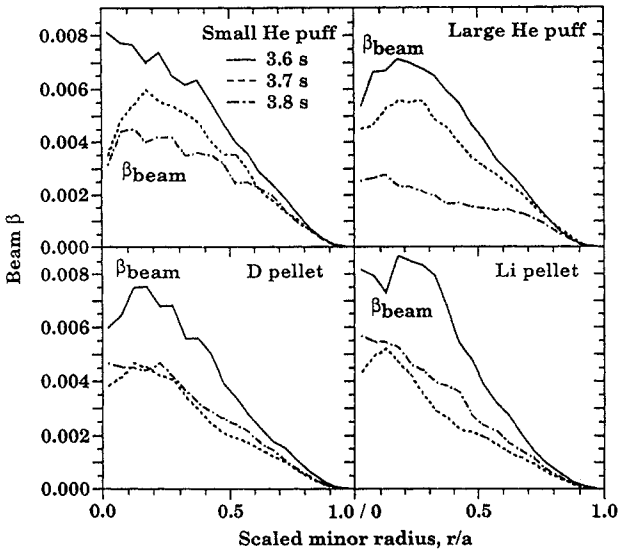

FIG. 9. Evolution of the beam beta profiles for the DT discharges in this experiment, as calculated by TRANSP. During the cooling perturbations the beam betas were reduced more than the alpha particle betas owing to the shorter beam thermalization time. These profiles include both the deuterium and the tritium beam components.

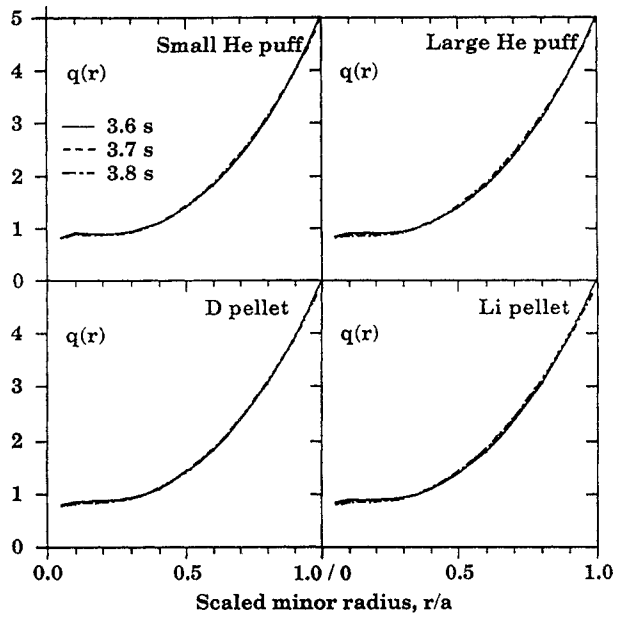

FIG. 10. Evolution of the q(r) *profiles as calculated by TRANSP for the four DT discharges in this experiment. The* q(r) *profiles did not change appreciably during the 0.2 s after the start of the cooling perturbations, owing to the long resistive relaxation time in these high temperature plasmas. The* q(r) *profiles were not measured during this experiment.*

For three of these DT discharges the maximum fusion power was in the range ≈ 5.0–5.5 MW, but the fourth (deuterium pellet) shot had only ≈ 3.5 MW of fusion power owing to an NBI source fault. No severe or unusual MHD activity occurred during the times of interest, but low level fishbone activity occurred before the cooling perturbations, as it did during the baseline DT discharge with no cooling perturbation, and sawtooth activity started ≥ 0.2 s after the start of the cooling perturbations (after the time of interest). For all four DT shots there was at least one companion DD discharge, which was used to help isolate the effect of alpha particles on the Alfvén frequency fluctuation spectra. The plasma parameters of the DD discharges were essentially the same as their companion DT discharges. Unless otherwise noted, the data described below are for the DT discharges.

TABLE II. SHOT LIST
(all shots at I = *2.0 MA,* R = *2.52 m (DT shots in bold))*

Shot	Shot type	NBI power (MW) at 3.6 s	$T_i(0)$ (keV) at 3.8 s	Peak neutron rate ($\times 10^{18}$/s)
75 923	Small He DD	26		< 0.03
75 926	Small He DT	28	15	1.8
75 930	Large He DD	25		< 0.05
75 932	Large He DT	29	8	1.8
75 934	D pel DD	27		< 0.07
75 936	D pel DT	27	12	1.2
75 938	Li pel DD	27		< 0.07
75 941	Li pel DT	29	11	1.9
73 268	Baseline	30	25	2.2
75 919	Baseline	27		< 0.03
75 922	Baseline	27		< 0.03

Machine and plasma parameters for these DT discharges and their DD comparison shots are shown in Table II. All discharges had I_p = 2.0 MA, R = 2.52 m and $P \approx$ 26–29 MW of NBI power from 3 to 4 s. The following sub-sections describe the plasma parameters and relevant measurements, in order to provide sufficient information for future TAE analyses.

4.1. Time evolution of plasma parameters

The time dependence of the line averaged electron density, the ion temperature, the DT neutron rate and the total stored energy during the cooling perturbations are shown in Fig. 2. The NBI power was applied from 3.0 to 4.0 s, and the cooling perturbations were started at 3.6 s. As expected, each type of cooling perturbation had a slightly different effect

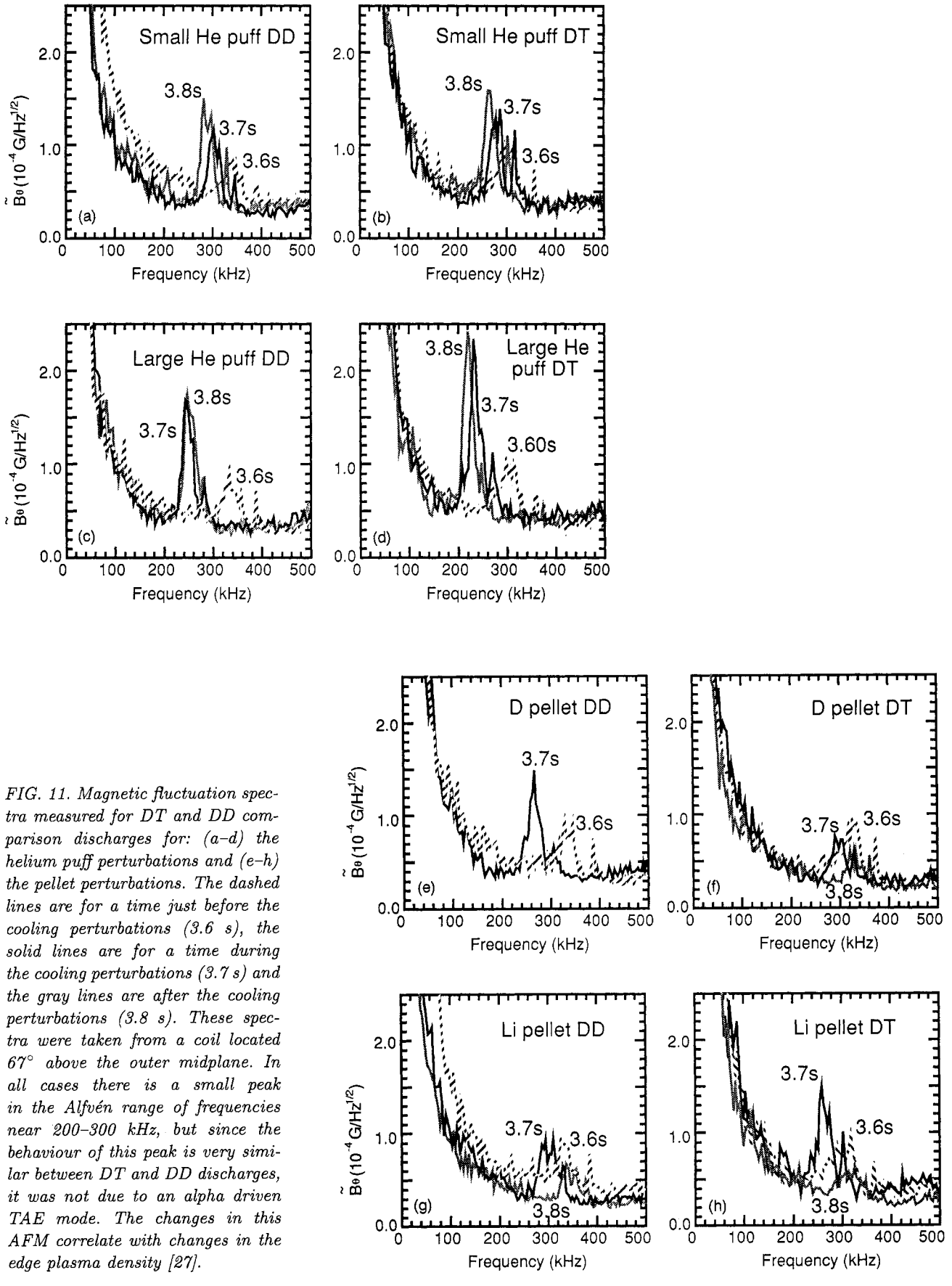

FIG. 11. Magnetic fluctuation spectra measured for DT and DD comparison discharges for: (a–d) the helium puff perturbations and (e–h) the pellet perturbations. The dashed lines are for a time just before the cooling perturbations (3.6 s), the solid lines are for a time during the cooling perturbations (3.7 s) and the gray lines are after the cooling perturbations (3.8 s). These spectra were taken from a coil located 67° above the outer midplane. In all cases there is a small peak in the Alfvén range of frequencies near 200–300 kHz, but since the behaviour of this peak is very similar between DT and DD discharges, it was not due to an alpha driven TAE mode. The changes in this AFM correlate with changes in the edge plasma density [27].

on the time evolution of the plasma parameters and profiles.

The small helium puff raised the line averaged density by ≈ 15% between 3.6 and 3.8 s, while the other perturbations raised it by ≈50% over this time. However, in all cases, the central electron density remained constant to within ≈ 10% during the time of interest (3.6 to 3.8 s), while the electron density profiles were broadened from supershot type (density peakedness ≈ 2.2) to L mode type (density peakedness ≈ 1.0–1.6). Profiles of the electron density evolution are shown in Fig. 3.

The small helium puff reduced the total plasma stored energy by ≈ 25% between 3.6 and 3.8 s, while the other perturbations reduced it by 30 to 40% during this time. This is roughly the expected change from supershot towards L mode confinement. The radial profiles of total plasma beta are also broadened towards the typical L mode profile shape, as shown in Fig. 4.

The time evolution of the measured ion temperature profiles is shown in Fig. 5 for these same four DT discharges. For the three cases with full NBI power, the measured central ion temperature dropped from $T_i(0) = 23 \pm 1$ keV to the range $T_i(0) =$ 8–15 keV within ≈ 0.2 s, while in the fourth (lower power) discharge it dropped from $T_i(0) = 19$ keV to $T_i(0) = 12$ keV. The central thermal ion beta, as shown in Fig. 6, decreased similarly to the central thermal ion temperature. However, the thermal ion beta did not significantly decrease outside $r/a \approx 0.5$, since the increase in ion density nearly balanced the decrease in T_i in this region.

The time evolution of the measured electron temperature profiles for these discharges is shown in Fig. 7. The electron temperature profile changed relatively little during these cooling perturbations, for example, from $T_e(0) = 9.0$–9.5 keV to $T_e(0) =$ 7–8 keV between 3.6 and 3.8 s. Sawteeth began at ≥ 3.8 s in most cases, i.e. just after the time of interest (see Section 4.5).

The alpha particle beta profile $\beta_\alpha(r)$, as shown in Fig. 8, was calculated by the time dependent TRANSP code using the DT neutron rate and the plasma parameters. The central alpha particle beta at the start of these cooling perturbations was comparable to the $\beta_\alpha(0) \approx 0.2\%$ calculated at the same time for the baseline DT case with 6.3 MW of fusion power (No. 73 268). The central alpha particle beta stayed nearly constant between 3.6 and 3.7 s, then decreased by ≈ 20–50% between 3.7 and 3.8 s, due to the decrease in the DT neutron rate and the alpha

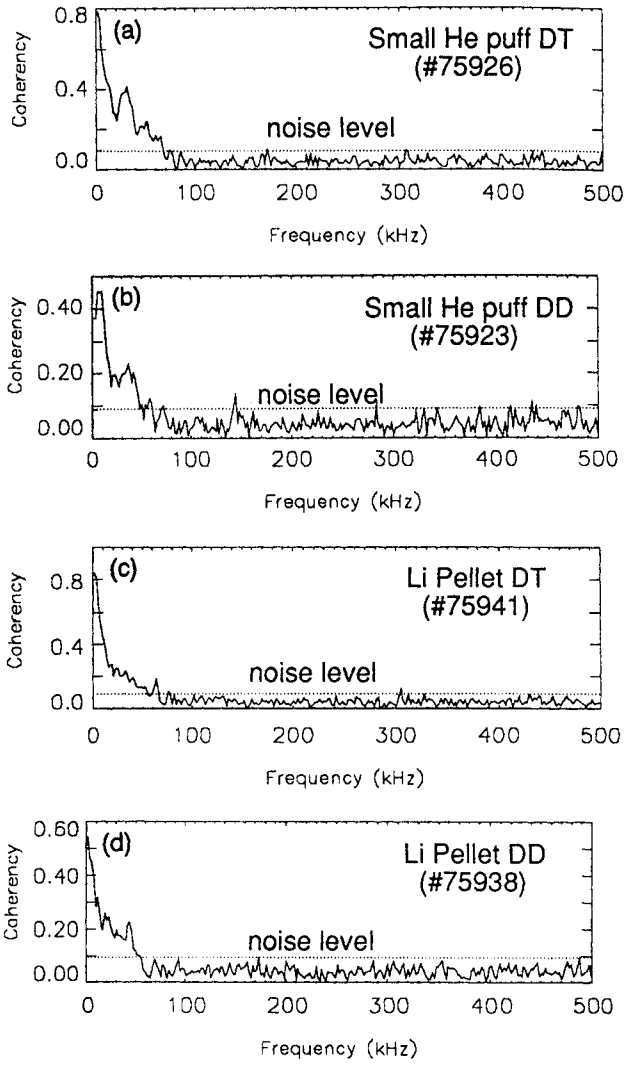

FIG. 12. Examples of BES coherency spectra during the cooling perturbations for (a, b) the small helium puff case and for (c, d) the lithium pellet case. There were no measurable coherent density fluctuations above 100 kHz in any of these DT or DD discharges. These cross-power spectra were centred at R = *323 cm* ($q \approx 2$) *with a radial separation of 5.5 cm and averaged over 3.6 to 3.9 s.*

thermalization. The shape of the $\beta_\alpha(r)$ profile stayed approximately constant, such that the location of the peak alpha particle pressure gradient remained constant at $r/a \approx 0.3 \pm 0.1$.

The beam beta profiles $\beta_b(r)$ calculated by TRANSP are shown in Fig. 9. These dropped by a factor of ≈ 2 between 3.6 to 3.8 s, owing to the relatively short beam thermalization time. Note that the beam beta was typically about 5 times higher than the alpha beta.

The $q(r)$ profiles calculated by TRANSP are shown in Fig. 10. The $q(r)$ profiles did not change

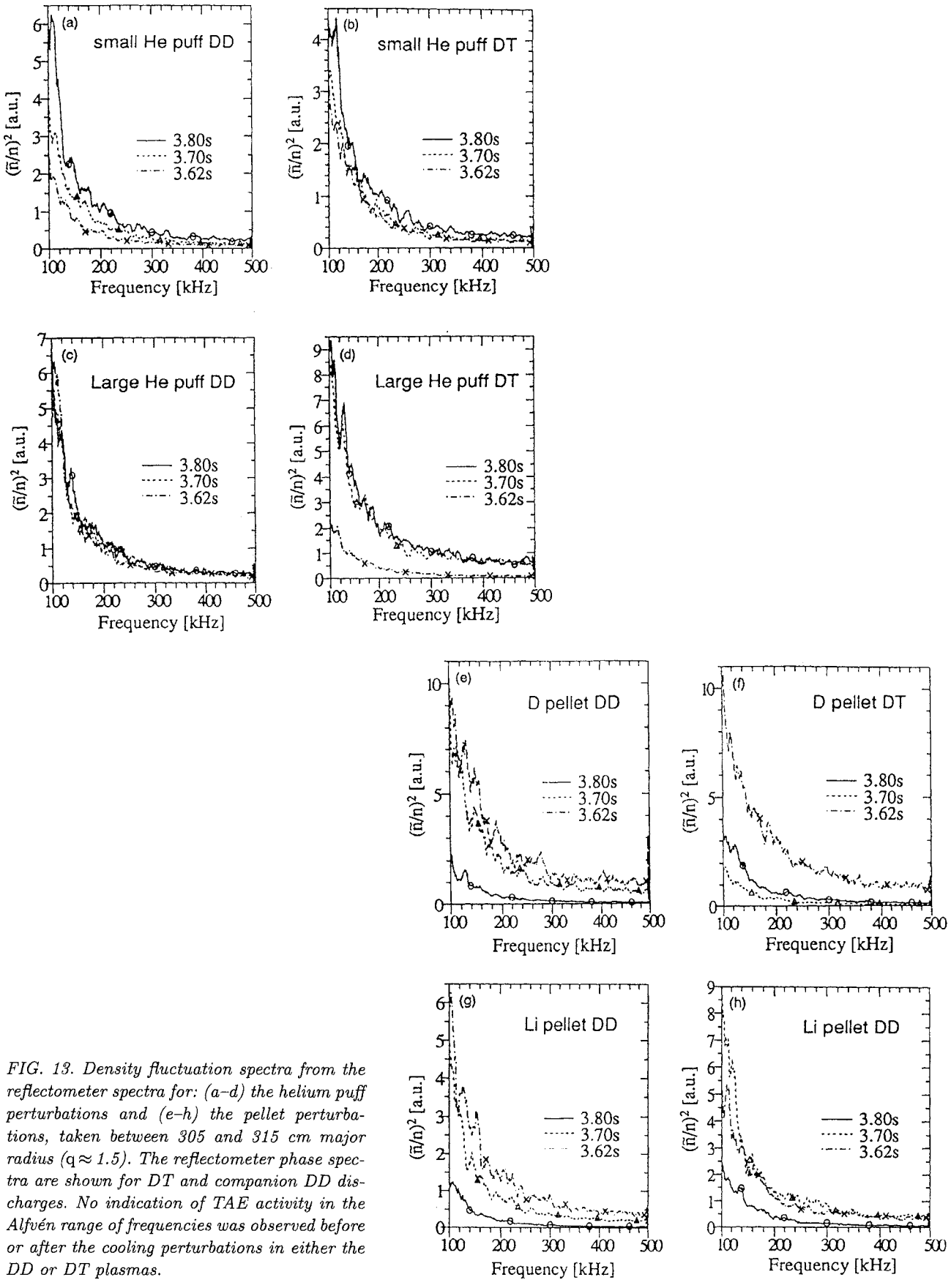

FIG. 13. Density fluctuation spectra from the reflectometer spectra for: (a–d) the helium puff perturbations and (e–h) the pellet perturbations, taken between 305 and 315 cm major radius ($q \approx 1.5$). The reflectometer phase spectra are shown for DT and companion DD discharges. No indication of TAE activity in the Alfvén range of frequencies was observed before or after the cooling perturbations in either the DD or DT plasmas.

significantly during the relatively short time-scale of interest for this experiment, as expected from the high electron temperature. Measurements of the $q(r)$ profile from the motional Stark effect (MSE) diagnostic were not available for these discharges. Measurements of $q(r)$ by the MSE on similar supershots perturbed by a helium puff show no change in $q(r)$ over these time-scales.

In summary, the intended scenario was obtained in at least three of the four DT discharges in this experiment, i.e. a transient reduction in ion temperature by about a factor of 2, along with a reduction in the alpha pressure by less than a factor of 2. These changes were made along with a broadening of the electron density profile, but relatively little change in the electron temperature profile, and without any significant increase in background plasma MHD activity (see Section 4.5). The theoretical analyses that explain the absence of TAE activity despite the lowered T_i are discussed in Sections 5 and 6.

4.2. High frequency magnetic fluctuation measurements

Measurements of the external magnetic fluctuations were made using magnetic loops with a frequency response of up to 500 kHz [26]. The resulting spectra of the edge poloidal magnetic fluctuations for the DT and comparison DD discharges are shown in Fig. 11. Each spectrum is averaged over ± 0.25 ms at three times of interest, i.e. before (3.6 s), during (3.7 s) and after (3.8 s) the cooling perturbations.

In almost all cases there was a small peak in the edge magnetic fluctuation spectrum at a frequency of $\approx$ 250–350 kHz. This peak was more than a factor of 10 times smaller than the TAE peaks seen during NBI or ICRH driven TAEs in TFTR DD plasmas [13, 26]. This peak occurred both before, during and after the cooling perturbations in both DD and DT plasmas. Since this feature behaved very similarly for DT and DD plasmas of a given type, these peaks cannot be ascribed to an alpha driven TAE mode (the super-Alfvénic fusion product pressure in the DD discharges is about a factor of $\approx$ 50 less than those in comparable DT discharges).

This small peak has been called an Alfvén frequency mode (AFM), since it occurs in the Alfvén frequency range. The origin of this peak is not understood, but it is not a TAE [27]. A systematic change in this AFM feature did occur during many of these cooling perturbations, for example, during the helium puffs its amplitude increased by a factor of 2 and its frequency decreased by $\approx$ 10%. However, these changes were similar for the DT and their DD comparison discharges, and so were not related to any alpha particle drive. The frequency of this peak was strongly correlated with the edge plasma density, and a similar feature also occurred in ohmic discharges without any fast ions present [27].

4.3. High frequency density fluctuation measurements

Measurements were made of internal density fluctuations in the frequency range up to 500 kHz using beam emission spectroscopy (BES) [28] and a microwave reflectometer [29]. No significant peaks in the TAE frequency range were seen for any of these discharges, in either DT or DD, implying that alpha driven TAEs were not observed in this experiment. These same diagnostics have observed NBI and ICRH driven TAEs in DD experiments [7, 26].

Examples of the coherence spectra of internal density fluctuations measured by BES for these discharges are shown in Fig. 12. These spectra were taken at a major radius of $R \approx 323$ cm, corresponding to $q \approx 2$ (the Shafranov shift was ≈ 15 cm) and averaged over 3.6 to 3.9 s. Cross-coherence spectra between two radii separated by 5 cm were used, which are more sensitive to coherent modes than simple auto-power spectra, since the incoherent noise in the spectra is reduced by averaging. Above 100 kHz no peaks were observed in any of the discharges above the statistical noise represented by a coherency at the 10% level. The upper limit to possible density fluctuations, assuming a 40 kHz bandwidth within $\approx$ 250–350 kHz, was $\delta n/n \approx$ 0.2–0.4%. This level is much smaller than that observed by BES during NBI driven TAE experiments [30]. Below 100 kHz, there were peaks corresponding to the usual low-n coherent MHD modes in both DT and DD discharges (Section 4.5).

Examples of internal density fluctuations measured by the reflectometer are shown in Fig. 13. These spectra were taken at major radii between $R = 305$ and 315 cm, corresponding to $q \approx 1.5$. Again, there were no observable coherent modes in the TAE frequency range above 200 kHz, although some modes below $\approx$ 150 kHz were observed in both DT and DD plasmas. These medium frequency modes are described elsewhere [31].

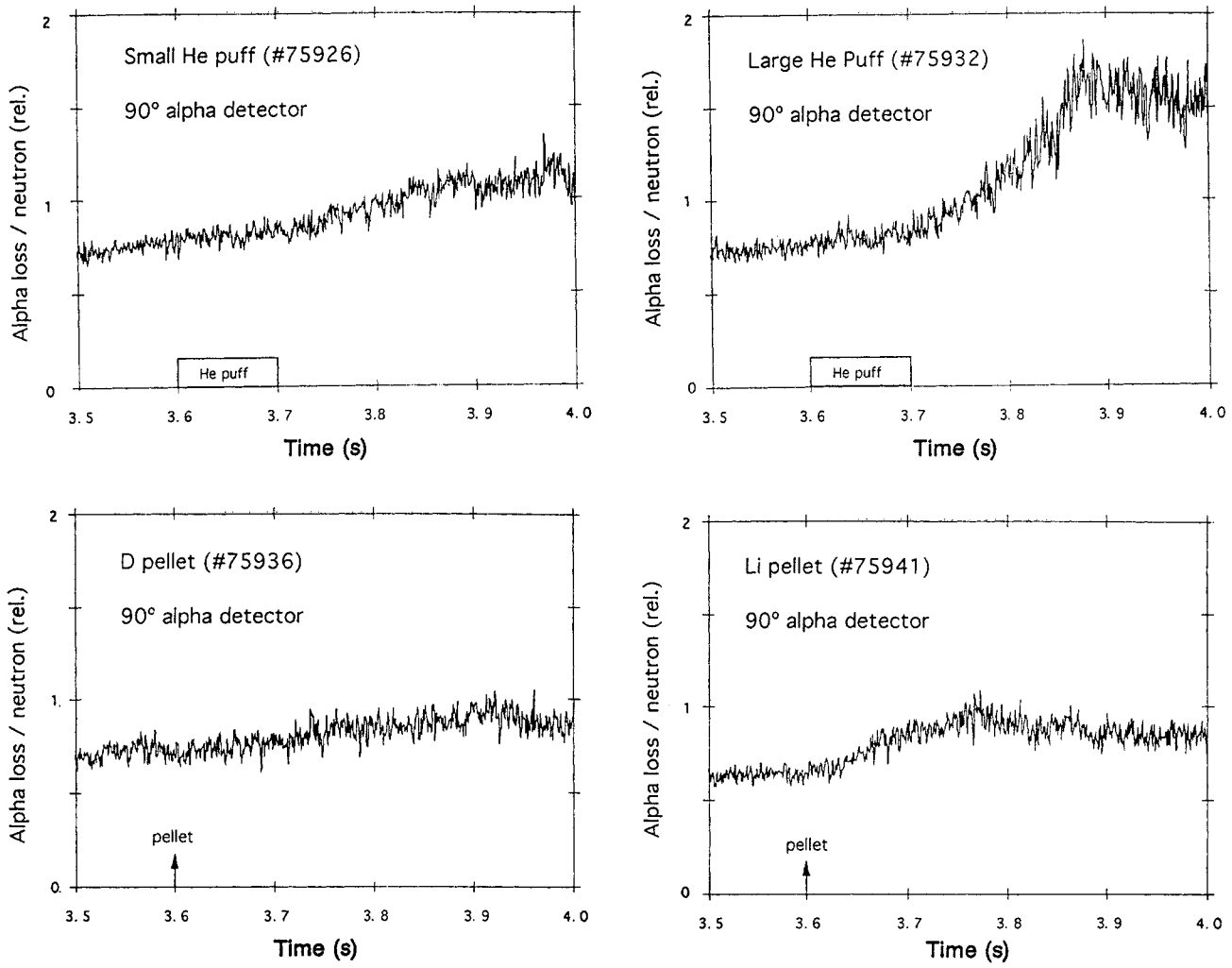

FIG. 14. Neutron normalized alpha particle loss signals measured by the lost alpha scintillator detector 90° below the outer midplane. In the large helium puff and lithium pellet cases, the alpha loss increased slowly during the cooling perturbation. However, this increase was due to the broadening of the alpha source profile, and not an excitation of alpha driven TAEs. A similar absence of alpha loss due to alpha driven TAEs is also observed on the other lost alpha detectors.

4.4. Alpha particle loss measurements

Measurements were made of alpha particle loss using the lost alpha scintillators [32]. The expectation was that an alpha driven TAE would cause anomalous alpha particle loss by moving passing alphas across the passing–trapped boundary to the lost alpha detector 90° below the outer midplane [33]. No measurements of the confined alpha population were available for these DT discharges.

The time dependence of the alpha loss to the 90° detector for the four DT discharges in this experiment is shown in Fig. 14. These signals were integrated over the pitch angle and gyroradius acceptance range of these detectors, and were normalized to the instantaneous DT neutron rate, after subtracting the neutron background.

In some of these DT discharges there was a gradual increase in the neutron normalized alpha loss during the cooling perturbations, with the largest of these increases occurring during the large helium puff case. This case is compared in Fig. 15 with expected first orbit loss, which was previously found to be the dominant component of alpha loss to this detector in the baseline DT discharges [34]. The measured increase of about a factor of 2 between 3.6 and 3.9 s agrees well with the expected increase in first orbit loss. This increase in first orbit alpha loss is due to the broadening of the neutron source profiles from supershot to L mode, which creates a larger alpha source on unconfined loss orbits (there was little change in the calculated $q(r)$ profile during this time). There is no sharp increase in the alpha loss at the lithium or

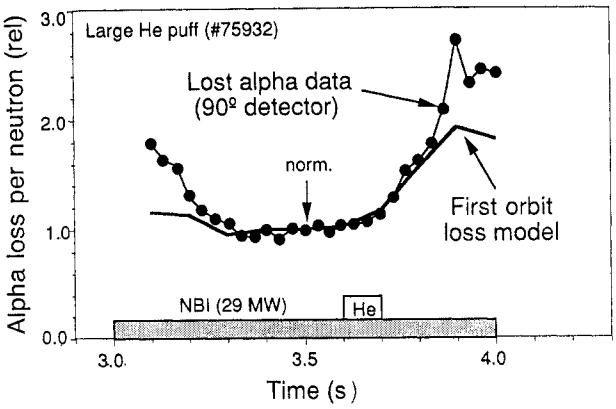

FIG. 15. Comparison of neutron normalized alpha loss in the 90° detector with the calculated first orbit loss for the large helium puff case. The increase observed between 3.6 and 3.9 s is explained by the broadening of the neutron source profile during the transition from a supershot to an L mode, and does not imply any alpha loss due to an alpha driven TAE. The uncertainties in the data and modelling are each ≈10 to 20% at all points.

deuterium pellet injection times.

Thus, there was no unexpected alpha particle loss observed during these cooling perturbations in the 90° lost alpha detector. In addition, there were no signs of anomalous alpha loss by the alpha loss in the 60 or 45° detectors (the 20° detector was not used in this experiment). There was also no time dependent change in the pitch angle or gyroradius distributions of alpha loss during these cooling perturbations, such as previously seen during MHD induced loss of DD fusion products [35]. Since the baseline DT discharge had a calculated global first orbit loss of ≈ 3%, the upper limit to any possible TAE induced loss is considerably less than 3%.

4.5. Other fluctuation measurements

Low frequency electron temperature and magnetic fluctuations were monitored by the electron cyclotron emission (ECE) and Mirnov diagnostics during both the DT and the DD comparison discharges. An example of these signals is shown in Fig. 16 for the large helium puff case in DT. The dominant fluctuations were $n = 1$ fishbones at $f \approx 5$ kHz, which were similar to those seen in the 6.3 MW baseline discharge [13, 26]. The edge magnetic perturbations from these fishbones were more than 1000 times larger than the perturbations due to the high frequency AFM, and generally decreased during the cooling perturbations. There were no sawteeth during the main time of interest for TAE stability between 3.6 and 3.8 s, but sawteeth began after 3.8 s in three of the four DT discharges in this experiment. Such sawtoothing is typical of TFTR L mode plasmas, and was not significantly different in the DD comparison discharges.

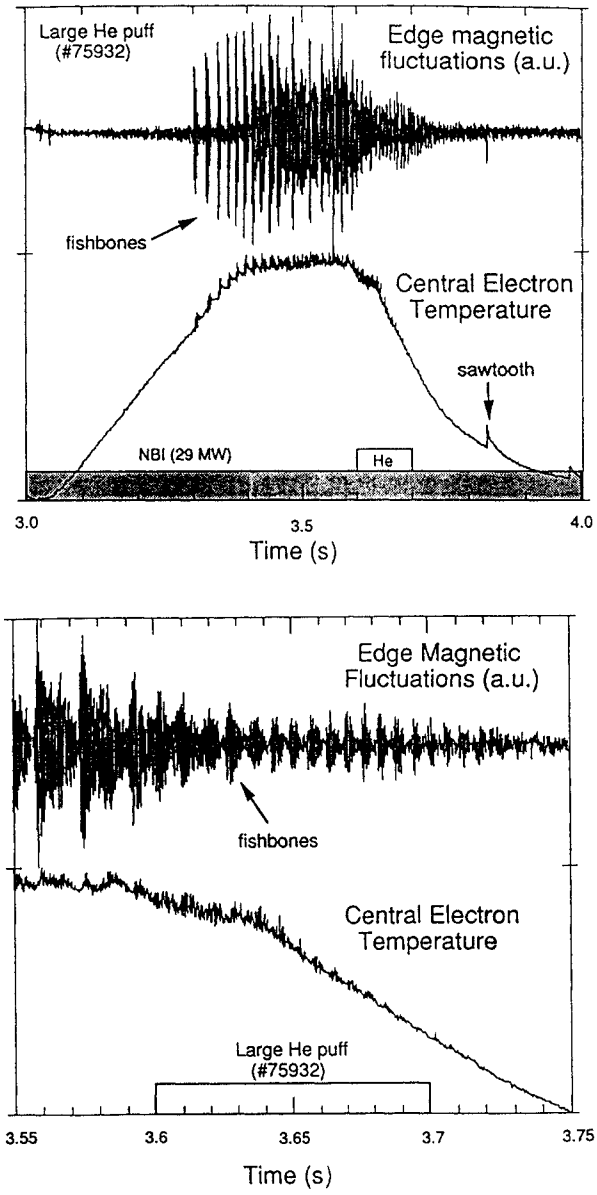

FIG. 16. Low frequency MHD activity during the large helium puff case, as measured by the ECE temperature diagnostic and the Mirnov magnetic pick-up loop. This and all the other discharges in this experiment had ≈ 5 kHz fishbone oscillations during NBI, which generally decreased in amplitude during the cooling perturbations. This MHD activity did not cause a measurable alpha particle loss, but may have caused an internal rearrangement of the alpha density profile (not measured in this experiment). Sawteeth appear only after 3.8 s in all of these discharges. Note the suppressed zero in the central electron temperature at 3.0 s.

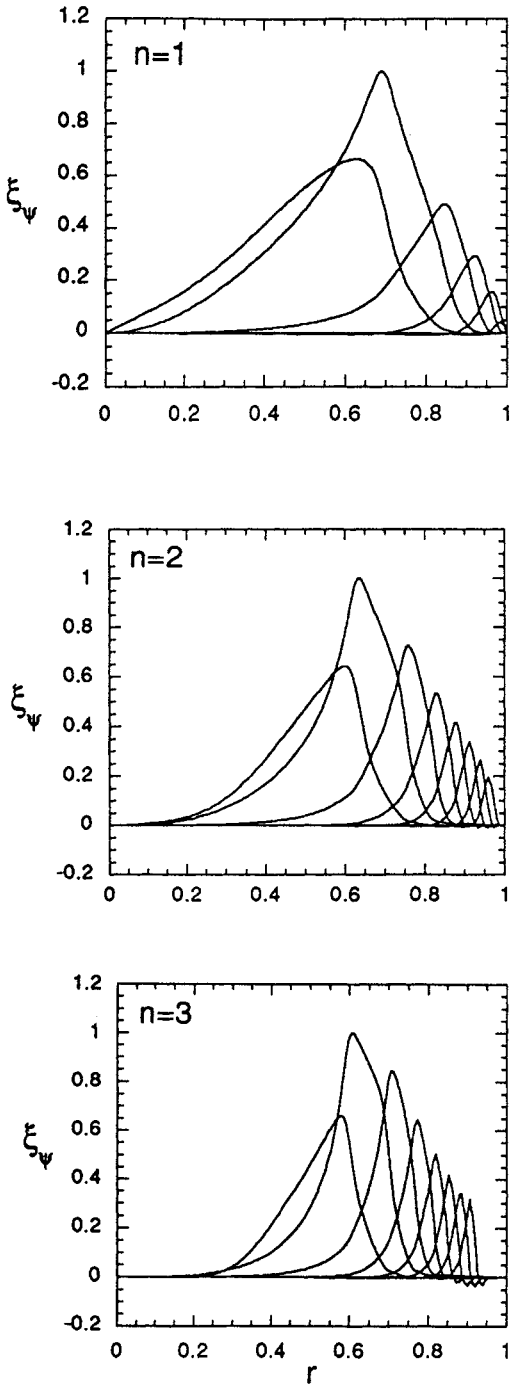

FIG. 17. TAE radial eigenmode structures for n = *1–3 just prior to the cooling perturbation for the small helium puff case, as calculated by the NOVA-K code (i.e. No. 75 926 at 3.6 s). The vertical axis in these plots is the relative displacement of the magnetic flux surfaces* ξ_Ψ *due to these eigenmodes for each* m *component at a given* n, *i.e.* $\xi\nabla\Psi$, *or* $r\xi_r$, *and the horizontal axis is the normalized minor radius. The TAE structures are mainly located in the outer half of the minor radius in these discharges, which is not optimal for coupling to the alpha particle pressure gradient, which is located near* r/a ≈ 0.3.

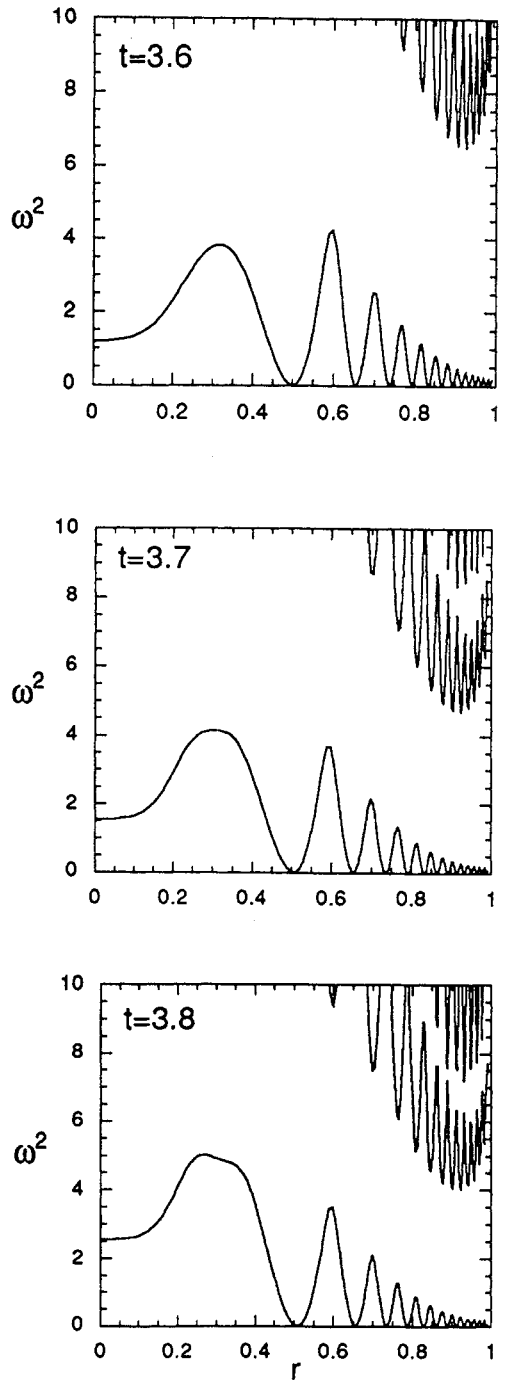

FIG. 18. TAE Alfvén frequency spectra at different times for the n = *3 mode for the small helium puff case (the frequencies are normalized to the Alfvén frequency, and the horizontal axes are normalized to the minor radius). The TAE gap mode exists just below the upper branch of the Alfvén continuum at 3.6 and 3.7 s, but moves into the Alfvén continuum and disappears at 3.8 s due to the change in density profile caused by the helium puff. The TAE frequency of* $(\omega/\omega_{TAE})^2 \approx 5$–$6$ *corresponds to* f $\approx$ *300 kHz.*

Another fluctuation measurement employed was edge ion cyclotron emission (ICE), in the frequency range up to ≈ 120 MHz. There was a significant increase in ICE during the helium puff perturbations, which is attributed to an alpha driven Alfvén cyclotron instability [36]. This increase in ICE is associated with an increased edge density due to the supershot to L mode transition, which causes the alphas passing through the plasma edge to become super-Alfvénic. This ICE is apparently not related to any alpha driven TAE.

5. TAE STABILITY ANALYSES

Theoretical TAE stability analyses were carried out for the helium puff discharges using the NOVA-K and TAE/FL codes (see Section 2). These analyses used the measured plasma profiles of $T_i(r)$, $T_e(r)$ and $n_e(r)$, along with the TRANSP analyses of derived profiles, such as $q(r)$ and $\beta_\alpha(r)$, as shown in Figs 3 to 10.

Since the formalism and approximations used in these two codes are substantially different, it is not surprising that they produce somewhat different results for a given case. In general, the NOVA-K code is most useful for marginal stability because of its perturbative nature, while the TAE/FL code is an initial value code most useful for calculating unstable cases with a finite growth rate. However, the end result was that both codes predicted the TAEs to be stable for low-n TAEs during these cooling perturbations.

A third TAE stability code has been used to analyse other TFTR DT discharges, namely the Candy–Rosenbluth code [37]. This code predicted that the baseline DT supershot (No. 73 268) was weakly unstable to TAEs with $n \leq 5$, and that electron curvature damping was the dominant damping mechanism, with thermal ion Landau damping being larger than beam ion Landau damping in this range. This code has not been used to analyse the cooling perturbations of this experiment. Note that all of these codes are fixed-boundary codes which treat internal modes, not free-boundary codes which include possible external modes [38].

5.1. TAE structure

The $n = 1$–3 TAE radial eigenmode structures as calculated by the NOVA-K code just before the cooling perturbations are shown in Fig. 17. These mode structures depend on the $n(r)$ and $q(r)$ profiles and the MHD equilibrium as derived from TRANSP. Each

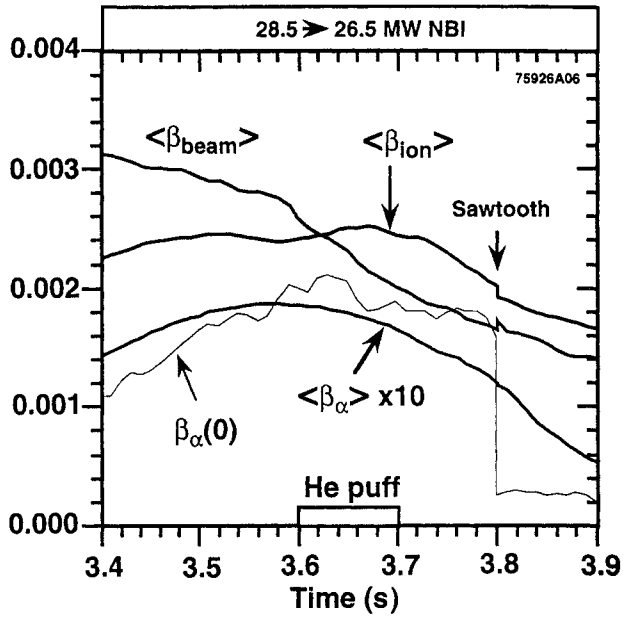

FIG. 19. Volume averaged toroidal betas versus time for the small helium puff case, as calculated by TRANSP. The volume averaged beam beta and thermal ion beta are comparable just before the cooling perturbation, and the beam beta decreases more than the thermal beta after the cooling perturbations. However, the beam ion beta is larger than the thermal ion beta at the location of the TAE resonances at r/a ≥ 0.5 (see Figs 6 and 9).

toroidal n number has a range of m numbers corresponding to various positions on the $q(r)$ profile; these different m modes are coupled by toroidal effects [1–4].

A crucial result from this analysis is that the TAEs were localized mainly in the outer half of the plasma, and tended to move closer to the outer edge as the n mode number increased from $n = 1$ to 3. This spatial location significantly reduced the alpha drive available for the TAE instability, since the alpha particle pressure gradient was localized near $r/a \approx 0.3 \pm 0.1$ (see Fig. 8). The TAEs of Fig. 17 are similar to those calculated for the 6.3 MW baseline discharge [12, 13], but different from the more recent $I = 2.5$ MA supershots, which had a broader pressure profile and a 'core localized' TAE mode [14].

In order for alpha particles to excite a strong TAE instability, the Alfvén continuous frequency spectrum should contain a 'gap' across the minor radius of the plasma at a frequency near $\omega_{TAE} \approx V_A/2qR$. In these experiments, the TAE gap structure for the $n = 1$ mode remained open during both the small and the large helium puffs, allowing the formation of a discrete mode at $r/a \approx 0.6$ and $\omega/\omega_A \approx 2$, i.e. at

$f \approx 300$ kHz. However, the $n = 2$ and $n = 3$ gap structures evolved significantly during these perturbations, as illustrated in Fig. 18 for the $n = 3$ mode in the small helium puff case, which 'disappeared' into the Alfvén continuum at 3.8 s, i.e. a TAE no longer existed inside the gap at this time due to the strong continuum damping. An even more rapid onset of continuum damping occurred for the large helium puff, according to the NOVA-K analysis.

These changes in the $n \geq 2$ TAE gap structures were an unanticipated side effect of the density perturbations that occurred during the helium puff cooling perturbations. Apparently, the increase in electron density at $r/a \approx 0.9$ caused a decrease in the local Alfvén speed and a decrease of the frequency of the upper branch of the Alfvén spectrum continuum. At the same time, the frequency of the lower branch of the Alfvén continuum increased in the region $r/a \approx 0.3$, further narrowing the gap. This closure of the TAE gap structure for $n \geq 2$ inhibited the formation of a TAE during the time when the ion temperature was lower. However, there were also other effects that contributed to the TAE stability, as discussed below.

5.2. NOVA-K modelling assumptions

The NOVA-K code [1, 2] is a non-variational kinetic MHD code that contains linear physics such as the ion and electron Landau damping, alpha particle drive and beam ion damping. The effects of continuum damping and radiative damping were not included in the present calculations.

The alpha particle distribution function in NOVA-K was modelled by a classical fast ion slowing down distribution for $E_\alpha \leq E_0 = 3.5$ MeV,

$$f(E_\alpha) \propto (E_\alpha^{3/2} + E_c^{3/2})^{-1} \quad (2)$$

The critical energy was assumed to be the standard steady state value of $E_c \sim 33T_e$. The assumed alpha energy distribution changed only through the variation of E_c with $T_e(r,t)$ during these discharges, and so did not explicitly include any non-steady state effects on the shape of the alpha distribution function as calculated by TRANSP [39, 40], for example, due to the sudden drop of the DT reaction rate during the cooling perturbations. The Doppler broadening of about ± 0.5 MeV around the alpha birth energy [41] was not included in this model.

The alpha pitch angle distribution was assumed to be isotropic, which is a fairly good approximation to the results of the Monte Carlo simulations, at least for alphas not too near the plasma edge [39, 40]. Alpha loss due to toroidal ripple effects was not included in this model for the alpha distribution, but constitutes only $\approx 10\%$ alpha energy loss for these plasmas [42]. Finite alpha particle and beam ion orbit effects are taken into account in the NOVA-K code. The finite banana orbit size and the shift of the alphas from the magnetic flux surfaces tend to reduce the alpha particle drive at a given alpha particle pressure [19].

The thermal ions were specified by the measured temperature $T_i(r,t)$ and the ion density profile as calculated by TRANSP, with an average ion mass of 2.5 for DT. There was a separate model for the beam ion component, with a beam density profile based on the TRANSP analysis, and an energy distribution of the

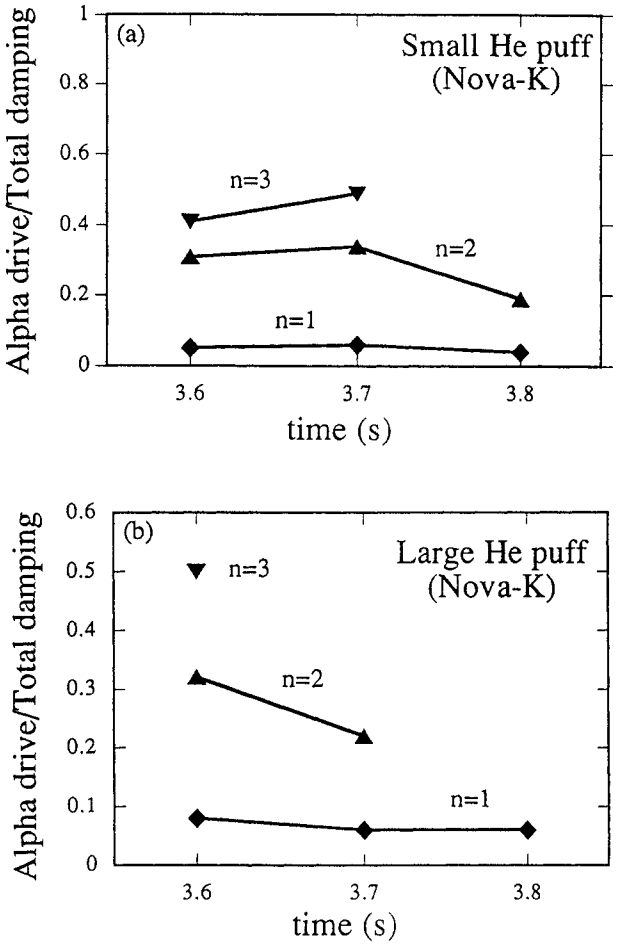

FIG. 20. Ratio of the alpha particle TAE drive to the total TAE damping for n = *1–3 modes, as calculated by NOVA-K for the (a) small and (b) large helium puff cases. This ratio is ≤1 for all cases, implying TAEs should be stable, which is consistent with the experimental results. The TAEs are slightly less stable just after the cooling perturbations at 3.7 s, but the alpha drive is still a factor of 2 lower than needed for TAE instability.*

beam ion species modelled by a classical steady state slowing-down distribution similar in form to Eq. (2), but with $E_c \sim 14T_e$. The beam energy component was assumed to be isotropic, which is a fairly good approximation for partially thermalized (but not full energy) beam ions [39, 40]. The relative populations and velocity distributions of co- and counter-injected deuterium and tritium ions are calculated separately from a TRANSP analysis for a particular discharge. Note that this separation between thermal and beam ion components was not made in the preliminary analyses of TFTR DT TAE stability (Section 2).

The beam and thermal ion Landau damping were calculated separately for each TAE n mode. Note that this calculation included the contribution of these ions to the TAE drive as well as to the damping, but in all cases the damping effect was far larger than the drive effect. The thermal ion Landau damping had a different radial dependence to the beam ion Landau damping, since the thermal ion beta profile was more peaked than the beam ion beta profile (see Figs 6 and 9).

At the beginning of the cooling perturbations the volume averaged thermal and beam ion betas were about equal, as shown in Fig. 19, but near the location of the low-n TAE structures (at $r/a \approx 0.6$) the beam beta was higher than the thermal ion beta. The injected beam ion speed was also closer to the $V_A/3$ resonance than the thermal ion speed (see Table I). Therefore, the beam ion damping dominated the thermal ion damping in the NOVA-K analysis.

5.3. NOVA-K TAE stability results

Time dependent TAE stability analyses were made using the NOVA-K code for the small and large helium puff cases, with the results shown in Table III and Fig. 20. The NOVA-K code calculated separately each driving and damping term, as listed in Table III. The resulting ratio of total alpha TAE drive to total TAE damping for $n = 1$–3 modes is shown in Fig. 20. The result was that all of these low-n TAEs were predicted to be stable both before, during and after these cooling perturbations.

The dominant damping mechanism in this analysis was the beam ion Landau damping, mainly due to the faster deuterium beams rather than the slower tritium beams [14]. Since the ratio of the beam speed to the Alfvén speed was close to 1/3 (Table I), the beam ion Landau damping also depended sensitively on the finite beam orbit size, which changed the effective parallel wavelength of the wave–particle resonance.

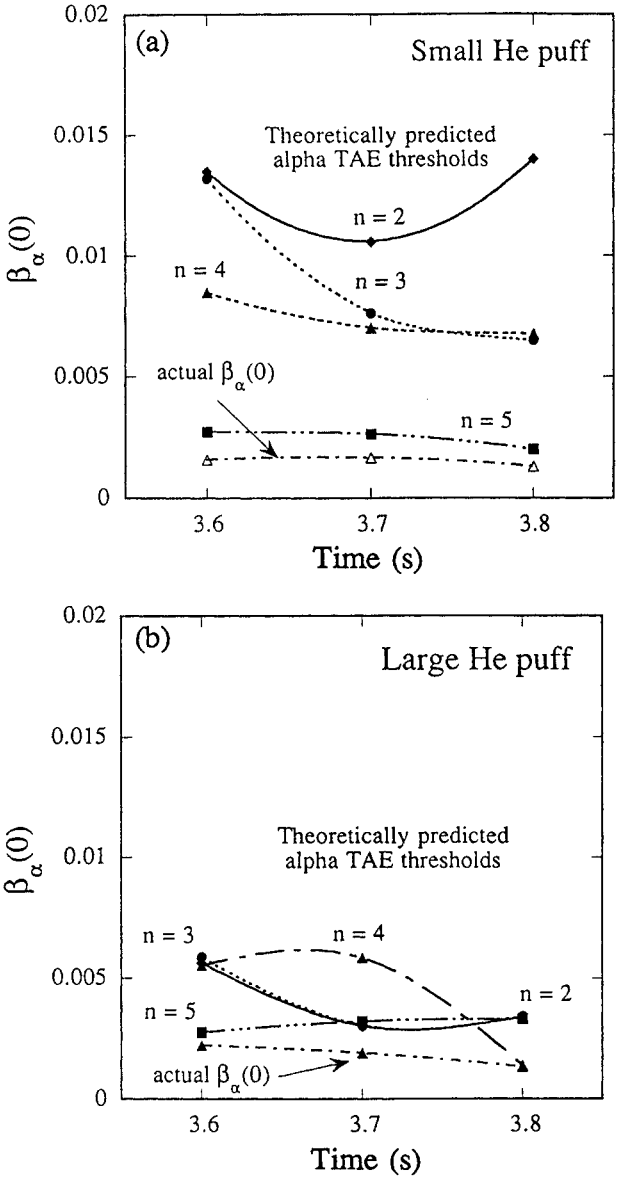

FIG. 21. Theoretically predicted β_α TAE thresholds versus time for the (a) small and (b) large helium puff cases as calculated by the TAE/FL code, along with the experimental β_α calculated for these cases by TRANSP. The alpha pressure profile is assumed to remain constant versus time as the central alpha particle beta varies. For all cases these discharges are predicted to be TAE stable, except perhaps for the n = 4 case at 3.8 s during the large helium puff, when the stability is marginal.

The finite orbit effect was found to increase the beam damping by up to a factor of 5 to 10 with respect to the zero orbit width case. Note that beam ion Landau damping for a slowing down distribution such as Eq. (2) is much larger than for an assumed Maxwellian distribution with the same average energy, since the contribution from the slope of $f(E_\alpha)$

TABLE III. TAE STABILITY ANALYSIS (NOVA-K)

Small He puff (No. 75 926)						Large He puff (No. 75 932)					
n = *1 mode*						n = *1 mode*					
Time	γ_{ILD}	γ_{ELD}	γ_{beam}	γ_α	$\gamma_\alpha/\gamma_{damp}$	Time	γ_{ILD}	γ_{ELD}	γ_{beam}	γ_α	$\gamma_\alpha/\gamma_{damp}$
3.6	0.14%	0.14%	0.69%	0.06%	0.05	3.6	0.21%	0.14%	0.78%	0.07%	0.08
3.7	0.15%	0.14%	0.97%	0.08%	0.06	3.7	0.11%	0.13%	1.6%	0.10%	0.06
3.8	0.02%	0.15%	1.16%	0.05%	0.04	3.8	0.1×10^{-4}	0.16%	0.86%	0.06%	0.06
n = *2 mode*						n = *2 mode*					
Time	γ_{ILD}	γ_{ELD}	γ_{beam}	γ_α	$\gamma_\alpha/\gamma_{damp}$	Time	γ_{ILD}	γ_{ELD}	γ_{beam}	γ_α	$\gamma_\alpha/\gamma_{damp}$
3.6	0.03%	0.15%	0.27%	0.14%	0.31	3.6	0.05%	0.14%	0.30%	0.14%	0.32
3.7	0.02%	0.14%	0.31%	0.16%	0.34	3.7	0.02%	0.14%	0.69%	0.18%	0.22
3.8	0.01%	0.16%	0.38%	0.10%	0.19	3.8	≫ the mode goes into continuum				
n = *3 mode*						n = *3 mode*					
Time	γ_{ILD}	γ_{ELD}	γ_{beam}	γ_α	$\gamma_\alpha/\gamma_{damp}$	Time	γ_{ILD}	γ_{ELD}	γ_{beam}	γ_α	$\gamma_\alpha/\gamma_{damp}$
3.6	0.02%	0.14%	0.30%	0.19%	0.41	3.6	0.08%	0.13%	0.39%	0.20%	0.50
3.7	0.02%	0.13%	0.30%	0.22%	0.49	3.7					
3.8	≫ the mode goes into continuum					3.8	≫ the mode goes into continuum				

Note: γ_{ILD} is ion thermal Landau damping, γ_{ELD} is electron Landau damping, γ_{beam} is beam ion Landau damping, γ_α is alpha drive and $\gamma_\alpha/\gamma_{damp}$ is alpha drive/total damping.

near the cut-off energy E_0 was large.

The thermal ion Landau damping was found to be sensitive to the mode number (i.e. mode structure), but was important only for the $n = 1$ mode (the mode considered in Ref. [1]). The thermal ion Landau damping was relatively small, particularly for $n \geq 2$, mainly because the TAEs in these discharges were localized in the outer half of the plasma where the ion beta was relatively low (see Figs 5 and 18).

After the helium puffs, the calculated thermal ion Landau damping did decrease as expected, but the beam ion Landau damping and the electron Landau damping were comparable to or larger than the thermal ion Landau damping, and were not significantly reduced by the helium puffs (electron collisional damping was found to be negligible). After the helium puff, the $n = 3$ mode disappeared into the Alfvén continuum, as illustrated in Fig. 18 for the small helium puff case.

It is interesting that the beam ion Landau damping in the small helium puff case actually increased between 3.6 and 3.8 s, even though the beam ion beta decreased (Figs 9 and 19). This was apparently due to the decrease in the Alfvén speed caused by the rise in density, which increased V_b/V_A and so increased the beam ion damping at the $V_A/3$ resonance.

The ratio of total alpha TAE drive to the total TAE damping increased with n-mode number, as shown in Fig. 20, and was ≈ 0.5 in the least stable ($n = 3$) case. This increase occurred because the electron damping and the beam ion damping were not sensitive to the n-mode number, whereas the alpha drive increased with the n-mode number. The conclusion from this analysis was that the experimental alpha beta was at least a factor of 2 below that needed theoretically to destabilize the TAEs in these discharges.

5.4. TAE/FL modelling assumptions

The TAE/FL code [3, 4] is based on a gyro-Landau fluid model for Alfvén frequency range instabilities. It is structured as an initial value fixed-boundary code with the Alfvén continuum built into the fluid equations [43]. This code is best utilized for calculating unstable cases with finite growth rates, whereas NOVA-K is most useful for marginal stability because of its perturbative nature. The wave fields calculated by the two codes are similar. The TAE/FL code can also be used to calculate non-linear effects, but this was not used for the present analyses.

In the TAE/FL analysis of these cooling perturbations the beam ions were assumed to have classical slowing-down distributions similar in form to that assumed in the NOVA-K code; however, the deuterium and tritium beam ions were lumped together in the TAE/FL code, whereas they are

treated separately in the NOVA-K code. The alphas are modelled using a Maxwellian distribution whose temperature is chosen to match a slowing-down distribution as closely as possible (since they are introduced by gyrofluid techniques). The finite gyroradius of the thermal ions is taken into account, but finite orbit effects are not taken into account for either the beam ions or the alpha particles.

The TAE/FL model also included thermal ion and electron damping effects, continuum damping, radiative damping [3] and a generalized resistivity, with the Alfvén continuum built into the fluid evolution equations. The balance of these damping terms against the alpha drive establishes the TAE threshold. The alpha pressure threshold for TAEs is evaluated by varying the central alpha beta (keeping the alpha profile shape constant). Individual driving and damping terms were not evaluated by this code.

5.5. TAE/FL code TAE stability results

Time dependent TAE stability analyses were also made using the TAE/FL code for the small and large helium puff cases, with the results shown in Fig. 21. In general, the TAE was predicted to be stable during these cooling perturbations. However, the $n = 4$ and 5 modes as analysed by TAE/FL were much closer to TAE instability, with one case being marginally unstable ($n = 4$ large helium puff at 3.8 s).

It is interesting that in the TAE/FL analysis the effect of beam ion Landau damping was not as significant as it was in the NOVA-K analysis, despite a similar model for the beam distribution function. This difference is discussed in Section 6.2.

6. DISCUSSION

This experiment was designed to test the theoretically predicted sensitivity of alpha driven TAEs to ion Landau damping. This was attempted by creating a large alpha population in TFTR DT discharges, and then transiently reducing the ion temperature and beta using helium puff or pellet cooling perturbations.

6.1. Summary of experimental results

The thermal ion temperature in DT supershots was successfully lowered from $T_i(0) \approx 20$ keV to $T_i(0) \approx 10$ keV in about 0.2 s, during which time the calculated alpha pressure was reduced by less than a factor of 2. However, no sign of any alpha driven TAEs was observed during any of these cooling perturbations. These modes were expected in the frequency range ≈ 300 kHz, but were not seen by either the external magnetic coils or the internal density fluctuation measurements. In addition, no anomalous alpha particle loss was observed in the alpha loss detectors.

TABLE IV. COMPARISON OF CALCULATED TAE STABILITY THRESHOLDS

			Experimental β_α (TRANSP)	
			Theoretical β_α for TAE mode	
Case	Time (s)	n	NOVA-K	TAE/FL
Small He	3.6	2	0.31	0.12
Small He	3.6	3	0.41	0.12
Large He	3.6	2	0.32	0.37
Large He	3.6	3	0.50	0.37
Small He	3.7	2	0.34	0.16
Small He	3.7	3	0.41	0.21
Large He	3.7	2	0.22	0.63
Large He	3.7	3	Continuum	0.63
Small He	3.8	2	0.19	0.09
Small He	3.8	3	Continuum	0.20
Large He	3.8	2	Continuum	0.38
Large He	3.8	3	Continuum	0.38

A small Alfvén frequency mode (AFM) was seen in the magnetic loops to increase during these cooling perturbations, but since these increases were very similar in DT and DD discharges, this mode could not have been driven by alpha particles. These AFMs have been found to be correlated with changes in the edge plasma density [27].

6.2. Summary of theoretical results

Two types of theoretical TAE stability analyses were made based on the experimental profiles and TRANSP runs. Both predicted that the alpha driven TAE should have been stable, despite the lowered thermal ion temperature. This is consistent with the observed absence of TAE instability in these discharges.

The theoretically predicted β_α threshold for TAE instability was typically a factor of 2 to 3 higher than the experimentally obtained β_α, as shown in Table IV (the 'experimental' value was derived from TRANSP

analysis based on the measured profiles). Only the $n = 2$ and $n = 3$ cases were calculated by both codes, and in most cases the two codes agreed to within about a factor of 2 to 3 in this ratio. Both codes predict that the calculated TAE stability should decrease with increasing n-mode number, at least for $n \leq 5$, mainly due to the increase in alpha drive with n.

However, there were some differences between the two codes, as might be expected from their different assumptions. For example, in the NOVA-K analysis the $n = 2$ and 3 modes moved into the Alfvén continuum at 3.7 and 3.8 s, implying that they were highly damped (NOVA-K did not calculate continuum damping explicitly). However, for the same cases the TAE/FL code did not show a substantial damping, even though it did include a model for continuum damping. This difference may be due to the sensitivity of the calculated TAE and gap structure to the assumed profiles, as illustrated in Fig. 18.

Perhaps the largest difference between these codes concerned the effect of beam ion Landau damping. Beam ion Landau damping dominated the total damping in the NOVA-K analysis, but was not significant in the TAE/FL analysis (as determined by turning it on and off). There are at least two possible explanations for this:

(a) Finite orbit effects are important (these were included in NOVA-K, but not TAE/FL).

(b) Non-perturbative effects are important (these are included in TAE/FL, but not NOVA-K).

The finite beam ion orbit effect was found to be significant in the NOVA-K code, where it increased the beam damping by a factor of 5 to 10, even though the beam ion orbit shift Δ of typically $\Delta/a \approx \rho_{\mathrm{pol}}/R$ was only about ± 5 cm for 100 keV passing beam ions at $r/a = 0.5$ at $I_{\mathrm{p}} = 2.0$ MA. The beam ion damping is very sensitive to this shift, since the beam ion speeds are near to the resonance at $V_{\mathrm{A}}/3$ (Table I), and the width of this orbit shift is comparable to the TAE width for the most unstable $n \geq 2$ modes. This effect was not included in the TAE/FL code.

The presence of non-perturbative effects included in the TAE/FL code imply that different damping mechanisms can interact. For example, if thermal ion Landau damping and beam ion Landau damping are suppressing the mode energy in the same ranges of poloidal mode number, then a non-perturbative calculation which takes this coupling into account is likely to show that both types of damping are less effective than in a perturbative calculation, which does not. In addition, inclusion of continuum damping and non-ideal effects such as ion gyroradius effects and resistivity can indirectly influence the effect of beam ion damping. These non-perturbative effects were not taken into account in the NOVA-K code.

Future calculations of TAE stability using NOVA-K should include the effect of radiative damping, which tends to increase with the toroidal n-number [14, 17]. This effect was not included in the present NOVA-K code owing to its perturbative approach, which considers only pure ideal MHD modes. Thus, the NOVA-K stability calculations somewhat underestimated the total damping and the necessary alpha beta for TAE instability.

6.3. Implications for future experiments

This experiment did not succeed in destabilizing the alpha-driven TAE, so further experimental work is needed in this area. Analysis of this experiment did raise several points that should be useful for future studies of alpha driven TAE instabilities:

First, these TAE stability analyses are evidently quite sensitive to small changes in the plasma profiles and equilibrium, as has been pointed out elsewhere [4, 18, 20, 23, 44]. This implies that future DT experiments should be based on analysis of very closely analogous DD comparison discharges. For the purposes of ITER TAE studies, this also implies that a broad range of possible profiles shapes and equilibria should be examined.

Second, it is necessary to have good DD comparison discharges to isolate clearly the alpha effects in DT plasmas. For example, the increases in the magnetic fluctuation spectra during the helium puffs (Fig. 11) could have mistakenly been attributed to an alpha particle driven effect if the corresponding DD comparison discharges (which also showed such an effect) were not available.

Third, a practical difficulty in these experiments was the unavoidable presence of background plasma MHD activity such as fishbones, which might have affected the TAE stability through an internal redistribution of the alpha particle pressure profile. Future experiments should try to measure directly the alpha profile in order to check the calculated alpha particle profiles.

Fourth, the methods used here for cooling the ions (helium puffs and pellets) were not optimal for reducing the ion Landau damping of TAEs, since most of the reduction in the ion beta was at $r/a \leq 0.5$

(Figs 6 and 9), whereas the higher-n TAE eigenfunctions were mostly outside $r/a \geq 0.5$ (Fig. 16). Ideally, experiments on TAEs should change the profiles of key parameters such as β_i and not just their magnitudes, although this is difficult in practice.

Some directions for future experiments were also brought out by the analysis of this experiment:

(a) A critical factor in TAE stability was the radial location of the alpha particle pressure gradient with respect to the radial eigenmode structure. The present experiment used a standard TFTR supershot scenario in which this location was not optimal for TAE instability, i.e. the low-n TAEs were located at $r/a \approx 0.6$, whereas the alpha particle pressure gradient was maximized at $r/a \approx 0.3$. Future experiments can be better designed to align these features, either by broadening the alpha pressure profile, or by changing the TAE structure by varying the $q(r)$ or $n(r)$ profiles [4]. Experiments on TFTR have already been done to search for TAEs excited when $q(0) > 1$, which should have a better alignment [45], and experiments on JT-60U have begun to control the hydrogen minority driven TAE using $q(r)$ and rotation control [44].

(b) An important factor brought out by this analysis was the potentially large effect of the beam ion Landau damping on TAE stability in TFTR. This suggests future experiments to study the post-beam phase of DT discharges when the alpha pressure remains high but the beam pressure drops significantly. So far there has been no evidence for TAE instability in this time period [11–13]. The beam ion Landau damping might also be reduced by lowering the beam voltage or by varying the beam species mixture [14].

(c) This analysis showed that the TAE instability should increase with the toroidal n-mode number. Future experiments should attempt to destabilize high-n alpha driven TAEs, which are relevant to ITER [10]. Additional measurements could also look for small scale TAE fluctuations, for example, using microwave scattering or reflectometry focused in the appropriate $q(r)$ range.

ACKNOWLEDGEMENTS

We thank R.J. Hawryluk, H.P. Furth, D.W. Johnson, K.M. McGuire, D.M. Meade and the TFTR Team for support for this work, which was performed under USDOE Contract No. DE-AC02-76CH03073.

REFERENCES

[1] CHENG, C.Z., et al., in Plasma Physics and Controlled Nuclear Fusion Research (Proc. 14th Int. Conf. Würzburg, 1992), Vol. 2, IAEA, Vienna (1993) 51.
[2] CHENG, C.Z., et al., in Plasma Physics and Controlled Nuclear Fusion Research (Proc. 15th Int. Conf. Seville, 1994), Vol. 3, IAEA, Vienna (1994) 373.
[3] SPONG, D.A., et al., ibid., p. 567.
[4] SPONG, D.A., et al., Nucl. Fusion **35** (1995) 1687.
[5] WONG, K.L., et al., Phys. Rev. Lett. **66** (1991) 1847.
[6] HEIDBRINK, W.W., et al., Nucl. Fusion **31** (1991) 1635.
[7] WILSON, R., et al., in Plasma Physics and Controlled Nuclear Fusion Research (Proc. 14th Int. Conf. Würzburg, 1992), Vol. 1, IAEA, Vienna (1992) 661.
[8] SAIGUSA, M., et al., Plasma Phys. Control. Fusion **37** (1995) 295.
[9] HAWRYLUK, R.J., et al., in Plasma Physics and Controlled Nuclear Fusion Research (Proc. 15th Int. Conf. Seville, 1994), Vol. 1, IAEA, Vienna (1995) 11.
[10] PUTVINSKI, S., et al., ibid., Vol. 2, p. 535.
[11] STRACHAN, J.D., et al., Phys. Rev. Lett. **72** (1994) 3526.
[12] McGUIRE, K.M., et al., Phys. of Plasmas **2** (1995) 2176.
[13] FREDRICKSON, E.D., et al., in Plasma Physics and Controlled Nuclear Fusion Research (Proc. 15th Int. Conf. Seville, 1994), Vol. 1, IAEA, Vienna (1995) 275.
[14] FU, G.Y., et al., Phys Rev. Lett. **75** (1995) 2336.
[15] FU, G.Y., VAN DAM, J.W., Phys. Fluids B **1** (1989) 1949.
[16] FURTH, H.P., et al., Nucl. Fusion **30** (1990) 1799.
[17] METT, R., MAHAJAN, S., Phys. Fluids B **4** (1992) 2885.
[18] STRAIT, E.J., et al., Nucl. Fusion **33** (1993) 1849.
[19] FU, G.Y., CHENG, C.Z., Phys. Fluids B **4** (1992) 3722.
[20] VILLARD, L., FU, G.Y., Nucl. Fusion **32** (1992) 1695.
[21] BIGLARI, H., CHEN, L., Phys. Rev. Lett. **67** (1991) 3681.
[22] CHU, M.S., et al., Phys. Fluids B **4** (1992) 3713.
[23] TURNBULL, A., et al., Phys. Fluids B **5** (1993) 2546.
[24] ZWEBEN, S.J., et al., Nucl. Fusion **28** (1988) 2230.
[25] SCOTT, S.D., et al., in 1992 International Conference on plasma Physics (Proc. Conf. Innsbruck, 1992), Vol 16C, Part I, European Physical Society, Geneva (1992) 39.
[26] FREDRICKSON, E.D., et al., in Controlled Fusion and Plasma Physics (Proc. 21st Eur. Conf. Mont-

pellier, 1994), Vol. 18B, Part I, European Physical Society, Geneva (1994) 246.
[27] CHANG, Z., et al., Nucl. Fusion **35** (1995) 1469.
[28] PAUL, S., FONCK, R.J., Rev. Sci. Instrum. **61** (1990) 3498.
[29] MAZZUCATO, E., et al., in Controlled Fusion and Plasma Physics (Proc. 22nd Eur. Conf. Bournemouth, 1994), Vol. 19C, Part IV, European Physical Society, Geneva (1995) 109.
[30] DURST, R., et al., Phys. Fluids B **4** (1992) 3707.
[31] NAZIKIAN, R., et al., Phys. Plasmas **3** (1996) 593.
[32] DARROW, D.S., et al., Rev. Sci. Instrum. **63** (1995) 476.
[33] SIGMAR, D.J., HSU, C.T., Phys. Fluids B **4** (1992) 1506.
[34] ZWEBEN, S.J., et al., Nucl. Fusion **35** (1995) 893.
[35] ZWEBEN, S.J., et al., Phys. Plasmas **1** (1994) 1469.
[36] CAUFFMAN, S., et al., Nucl. Fusion **35** (1995) 1597.
[37] CANDY, J., ROSENBLUTH, M.N., Nucl. Fusion **35** (1995) 1069.
[38] VILLARD, L., et al., Nucl. Fusion **35** (1995) 1173.
[39] BUDNY, R.V., Nucl. Fusion **34** (1994) 1247.
[40] BUDNY, R.V., et al., Nucl. Fusion **35** (1995) 1497.
[41] SADLER, G.J., VAN BELLE, P., in Controlled Fusion and Plasma Physics (Proc. 22nd Eur. Conf. Bournemouth, 1995), Vol. 19C, Part II, European Physical Society, Geneva (1995) 269.
[42] REDI, M.H., et al., ibid., p. 105.
[43] SPONG, D.A., et al., Phys. Plasmas B **4** (1992) 3316.
[44] KIMURA, H., et al., J. Plasma Phys. Fusion Res. **71** (1995) 1147.
[45] BATHA, S.H., et al., Nucl. Fusion **35** (1995) 1463.

(Manuscript received 14 September 1995
Final manuscript accepted 2 February 1996)